Modeling, simulation and experimental verification of the trajectory and breakup of a particle laden spiraling liquid jet

S. Gramlich*, M. Piesche
University of Stuttgart, Institute for Mechanical Process Engineering,
Böblinger Strasse 72, 70199 Stuttgart
gramlich@imvt.uni-stuttgart.de and piesche@imvt.uni-stuttgart.de

Abstract

The breakup of a particle laden viscous liquid jet, emitted from a cylindrical nozzle in a rotating cup and thus elongated by centrifugal force is studied by means of perturbation theory and experiments. In perturbation theory the flow of the jet is decomposed into a steady state motion and the transient motion of the small perturbations visible by the oscillation of the jet radius, which leads to breakup. The steady state equations of motion providing the contour as well as the trajectory of the unperturbed jet are derived by balances of forces and mass. The influence of the surrounding gas atmosphere is included. The transient motion of the perturbations is studied by means of linear stability analysis. The equations of motion for the particle laden liquid jet are based on balances of mass and impulse in the Eulerian formulation. Hence each phase is treated as a continuum. The pressure oscillation in the surrounding gas is considered by treating the gas motion as potential flow. Both, temporal and spatial stability analysis is implied. Jet stability is also investigated experimentally. The curvature, breakup length and the resulting drops are analyzed using shadow imaging. The experimental findings are compared to the numerical model.

Introduction

In many industrial applications like prilling, spray drying or spray coating rotating disc atomizers are used to disintegrate droplets of a liquid that can be particle laden. Operating the atomizer in the regime of Rayleigh type drop formation leads to drop sizes that are narrowly distributed.

The linear stability analysis of the Rayleigh [16] type disintegration of straight and cylindrical liquid jets have been addressed amongst others by [19, 2, 8]. The non linear stability analysis including secondary breakup of satellite droplets have been investigated by [13] and [1]. The instability of viscous jets elongated by gravity has been addressed amongst others by [11] whereas [5] and [10] additionally accounted for a gas motion normal to the nozzle axis. Piesche [12] derived a physical-mathematical model to analyze cylindrical particle laden liquid jets.

The instability of spiraling liquid jets with Newtonian or non-Newtonian flow properties have been addressed amongst others by [9, 18, 14, 3, 4].

For the determination of the resulting drop size, the exact time steady solution of the radius at the point of breakup is necessary, since the drop has the same volume as the cylindrical piece of jet with the wavelength λ and the local steady jet radius $\bar{r}_j$. The equation of motion describing the time steady motion of the jet is under-determined. Sauter [17] found a method to solve this equation for the contour of vertical jets exposed to gravity.

For the breakup and drop formation of particle laden spiraling liquid jets no sufficient experimental or numerical fundamentals can be found. The knowledge about the influence of a disperse and highly concentrated phase on the breakup behavior rely on product specific experienced data and are gained by empirical studies. Physical-mathematical models as well as numerical methods to predict the drop diameter for Rayleigh type disintegration of particle laden spiraling liquid jets are missing.

The objective of this work is to derive a model to predict the drop size from Rayleigh type disintegration as a function of particle size and concentration. The analysis include temporal as well as spatial stability behavior. Besides the theoretical modeling, experimental investigation is presented, to prove the accuracy of the physical model.

Physical Model

The physical model is based on the drawing in figure 1. It shows the contour of an oscillating phase interface of a liquid jet which is spiraling with the curvature k around a cylinder with radius n_0 rotating with the angular velocity ω. The jet is assumed to be rotationally symmetric. The liquid contains particles with diameter d_p of volume concentration ϵ_s and emerges from a cylindrical nozzle with radius r_0 with the velocity w_0. Due to

*Corresponding author: gramlich@imvt.uni-stuttgart.de

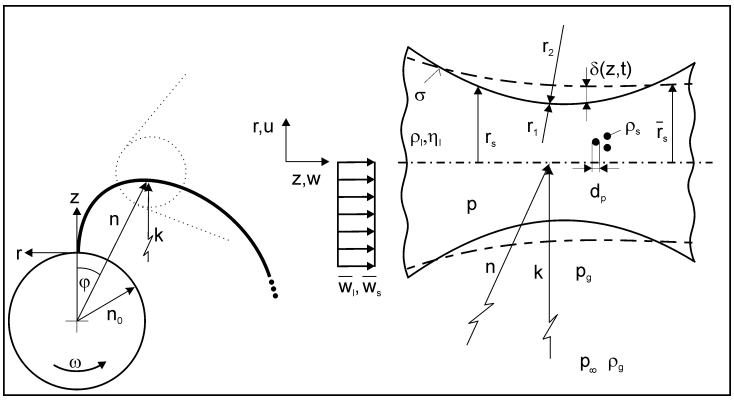

Figure 1. Physical model.

centrifugal forces the axial velocity $\bar{w}_l$ increases and because of mass conservation, the jet radius $\bar{r}_j$ decreases (dashed line) along the jet. The solid particles are moving with the same velocity as the liquid $\bar{w}_s = \bar{w}_l = \bar{w}$. The motion of the gas phase surrounding the rotating atomizer is treated as potential flow.
The equations of motion of the jet are derived in a cylindrical coordinate system r, z with the origin in the nozzle orifice. The axial coordinate is congruent with the jet axis. The curvature of the jet is considered to be small, thus along a balanced jet segment the coordinate system is cylindrical. The global coordinate system n, φ is also cylindrical but stationary with the origin in the rotation axis of the rotating atomizer. The liquid has the viscosity η_l and the density ρ_l, the solid particles have the density ρ_s and the gas has the viscosity η_g and the density ρ_g respectively. On the interface between the liquid and the gaseous phase acts the surface tension σ.
Because of small disturbances on the jets surface, the jet radius r_j changes locally and temporally. Thus, the motion of the liquid, solid and gaseous phase can be split up into a time independent basic motion describing the contour and trajectory of the liquid jet and a time dependent oscillation induced by capillary forces which grow along the jet and lead to breakup. Therefore, the jet radius r_j can be decomposed as

$$r_j(t,z) = \bar{r}_j(z) + \delta(z,t) \tag{1}$$

with a time steady jet radius $\bar{r}_j$ and a transient oscillation of the jets' surface $\delta(z,t)$.
Therefore, the velocities and pressures are also decomposed :

$$w_k(t,z) = \bar{w}_k(z) + w'_k(t,z) \tag{2}$$
$$u_k(t,z) = \bar{u}_k(z) + u'_k(t,z) \tag{3}$$
$$p(t,z) = \bar{p}(z) + p'(t,z) \tag{4}$$
$$p_g(t,z) = p_\infty + p'_g(t,z) \tag{5}$$

with the time steady quantities $\bar{w}_k$, $\bar{u}_k$ for the axial and normal velocity and $\bar{p}$ the pressure inside the jet as well as the perturbed quantities w'_k, u'_k, p' and p'_g. The index k stands for either gas, liquid or solid $k = g, l, s$.

In the following, the time steady motion of a spiraling liquid jet is presented and then the stability analysis is shown, giving the critical wave number of the jet breakup.

Time steady motion

The time steady motion of a spiraling liquid jet is investigated by balancing forces on an infinitesimal jet segment. The following assumptions had to be made, to reduce the problem to a manageable amount:

- The motion of the jet is uniaxial stretching
- No shear stresses act neither on the phase interface nor in the cross section of the jet
- The suspension is treated as one continuous phase, the viscosity follows a viscosity law $\eta = f(\dot{\gamma})$ and has an averaged density $\rho = \epsilon_s \rho_s + (1 - \epsilon_s)\rho_l$
- The particle concentration is constant in time and space. The particles move without slip, thus $\bar{w}_s = \bar{w}_l = \bar{w}$.

- The surrounding gas phase has the pressure p_∞, the relative gas motion is defined by $\bar{v}_{g,rel}$ and has a local inclination angle of ζ relative to the jet.

The acting forces are inertial force, viscous force, pressure force, surface tension force, centrifugal force, Coriolis force and drag force. The balance results in the equations of motion in axial direction:

$$\bar{W}\frac{d\bar{W}}{dZ} - \frac{1}{We}\frac{\rho_l}{\rho}\frac{1}{\bar{R}_j^2}\left(\frac{d\bar{R}_j}{dZ}\right) - \frac{3H}{Re}\frac{\rho_l}{\rho}\frac{1}{\bar{R}_j^2}\frac{d}{dZ}\left(\bar{R}_j^2\frac{d\bar{W}}{dZ}\right) - RoN\sin\alpha + \frac{\rho_g}{\rho}\frac{c_{D,lg}}{\pi\bar{R}_j}\bar{V}_{g,rel}^2\cos\zeta = 0 \tag{6}$$

and normal to the jets axis:

$$\frac{\bar{W}^2}{K} + RoN\cos\alpha - 2\bar{W}\left(\frac{Ro}{D}\right)^{\frac{1}{2}} - \frac{\rho_g}{\rho_l}\frac{c_{D,lg}}{\pi\bar{R}_j}\bar{V}_{g,rel}^2\sin\zeta = 0 \tag{7}$$

with the dimensionless time steady axial velocity $\bar{W} = \frac{\bar{w}}{w_0}$, the relative gas velocity $\bar{V}_{g,rel} = \frac{\bar{v}_{g,rel}}{w_0}$, the dimensionless jet radius $\bar{R}_j = \frac{\bar{r}_j}{r_o}$ the dimensionless axial coordinate $Z = \frac{z}{r_o}$, the position vector $N = \frac{n}{n_o}$, the radius of the curvature $K = \frac{k}{r_0}$, the drag coefficient $c_{D,lg}$, the inclination angle α and the angle of incidence of gas motion ζ as well as the characteristic numbers: the Weber number $We = \frac{\rho_l r_0 w_0^2}{\sigma}$, the Reynolds number $Re = \frac{\rho_l r_0 w_0}{\eta_l}$, the rotation number $Ro = \frac{\omega^2 r_0 n_0}{w_0^2}$, the diameter ratio $D = \frac{n_0}{r_0}$, the viscosity ratio $H = \frac{\eta}{\eta_l}$, the density ratio gas/liquid $\frac{\rho_g}{\rho_l}$ and the density ratio suspension/liquid $\frac{\rho}{\rho_l}$. The shear thinning behaviour of the viscosity of a particle laden liquid expressed by the Carreau-Yasuda model which results in the function $H = 1 + (H_0 - 1)\left[1 + (\lambda\dot{\gamma})^a\right]^{\frac{n-1}{a}}$ with the time constant λ, the strain rate $\dot{\gamma}$, the power law exponent n and the dimensionless parameter a. For Newtonian behavior the viscosity function reduces to unity, $H = 1$.
The relative gas velocity is composed from the absolute jet motion and the gas motion induced by the rotating cup atomizer which is expressed assuming potential flow around the cylinder, $\bar{v}_g = \omega n_0^2/n$. The relative velocity becomes therefore

$$\bar{V}_{g,rel} = \sqrt{\bar{W}^2 + RoDN^2\left(1 - N^{-2}\right)^2 - 2\bar{W}\sqrt{RoD}N\left(1 - N^{-2}\right)\cos\alpha} \tag{8}$$

and the angle of incidence

$$\tan\left(\frac{\pi}{2} - \zeta\right) = \frac{\bar{W} - \sqrt{RoD}\,N\left(1 - N^{-2}\right)\cos\alpha}{\sqrt{RoD}\,N\left(1 - N^{-2}\right)\sin\alpha}\,. \tag{9}$$

The drag coefficient $c_{D,lg}$ for an inclined cylindrical jet segment was defined by means of direct numerical simulation (DNS) of the jet. Equation (6) is an ordinary differential equation of second order with only one starting condition known, which is the axial velocity of the jet at the orifice $\bar{W}|_{Z=0} = 1$. The gradient in axial direction serving as the second boundary condition $\frac{d\bar{W}}{dZ}|_{Z=0}$ is not accessible. The problem can be solved applying the method of [17] to the presence of a centrifugal field, which had been presented in earlier studies [7, 6, 4]. The calculation of the axial velocity described above is coupled with equation (7) for the radius of curvature K, equation (8) and (9) for the relative gas motion and a set of equations for the radial position N, the angular coordinate φ and the inclination angle α:

$$\frac{dN}{dZ} = \frac{\sin\alpha}{D} \tag{10}$$

$$\frac{d\varphi}{dZ} = \frac{\cos\alpha}{ND} \tag{11}$$

$$\frac{d\alpha}{dZ} = \frac{\cos\alpha}{ND} - \frac{1}{K}. \tag{12}$$

This set of equations (7-12) determines the time steady motion of a spiraling liquid jet. The influence of the surrounding gas is included by the drag force.

Stability Analysis

The investigations of the perturbations visible by the oscillating jet radius are based on Navier-Stokes-Equations in cylindrical coordinates r, z, θ. Due to the assumption of rotational symmetry, the derivatives with respect to the angular coordinate θ vanish. The equations of motion for particle laden liquid flow are given in Eulerian formulation. Hence, each phase is treated as a continuum and the coupling of the liquid and solid phase is given by the interaction terms in the equations for impulse. A drag coefficient for the particles is defined postulating creeping flow around the spherical particles.

The theory implies the assumption that the single phases are influenced by random or forced disturbances which are either growing or damped depending on the liquid, solid and gaseous properties and the geometric and operating conditions. According to perturbation theory, the flow is decomposed into a time steady motion and the transient motion of the disturbances showing oscillations of the jets interface. From the decomposition the Navier-Stokes-Equations result in the linear perturbation equations for the liquid phase:

$$\frac{\partial U_l'}{\partial R} + \frac{U_l'}{R} + \frac{\partial W_l'}{\partial Z} = 0 \tag{13}$$

$$\frac{\partial U_l'}{\partial T} + \bar{W}\frac{\partial U_l'}{\partial Z} = -\frac{\partial P'}{\partial R} + \frac{1}{Re}\left(\frac{\partial^2 U_l'}{\partial R^2} + \frac{1}{R}\frac{\partial U_l'}{\partial R} - \frac{U_l'}{R^2} + \frac{\partial^2 U_l'}{\partial Z^2}\right) + \frac{18}{Re}\frac{\epsilon_s}{D_p^2}(U_s' - U_l') \tag{14}$$

$$\frac{\partial W_l'}{\partial T} + \bar{W}\frac{\partial W_l'}{\partial Z} = -\frac{\partial P'}{\partial Z} + \frac{1}{Re}\left(\frac{\partial^2 W_l'}{\partial R^2} + \frac{1}{R}\frac{\partial W_l'}{\partial R} + \frac{\partial^2 W_l'}{\partial Z^2}\right) + \frac{18}{Re}\frac{\epsilon_s}{D_p^2}(W_s' - W_l') \tag{15}$$

and for the solid phase:

$$\frac{\partial U_s'}{\partial R} + \frac{U_s'}{R} + \frac{\partial W_s'}{\partial Z} = 0 \tag{16}$$

$$\frac{\partial U_s'}{\partial T} + \bar{W}\frac{\partial U_s'}{\partial Z} = -\frac{\rho_l}{\rho_s}\frac{\partial P'}{\partial R} + \frac{18}{Re}\frac{\epsilon_s}{D_p^2}\frac{\rho_l}{\rho_s}(U_l' - U_s') \tag{17}$$

$$\frac{\partial W_s'}{\partial T} + \bar{W}\frac{\partial W_s'}{\partial Z} = -\frac{\rho_l}{\rho_s}\frac{\partial P'}{\partial Z} + \frac{18}{Re}\frac{\epsilon_s}{D_p^2}\frac{\rho_l}{\rho_s}(W_l' - W_s')\ . \tag{18}$$

The solution of the set of partial differential equations (13-18) requires the specification of boundary conditions. At the liquid/gas interface the pressure drop due to the oscillation of the jets interface is given by

$$P' = P_g' + \frac{2}{Re}\frac{\partial U_l'}{\partial R} - \frac{1}{We}\left(\frac{\Delta}{\bar{R}_j^2} + \frac{\partial^2 \Delta}{\partial Z^2}\right) \tag{19}$$

with the dimensionless radial displacement $\Delta = \frac{\delta}{r_0}$. The radial velocity of the disturbance at the jet radius $U_l'|_{R=R_j}$ equals the motion of the radial displacement:

$$U_l' = \frac{\partial \Delta}{\partial T} + \bar{W}\frac{\partial \Delta}{\partial Z}. \tag{20}$$

The shear stress at the interface is zero:

$$\frac{\partial W_l'}{\partial R} + \frac{\partial U_l'}{\partial Z} = 0. \tag{21}$$

For solving a set of partial differential equations describing an oscillation a suitable separation approach is

$$U_k' = \hat{U}_k(R)\exp\left[i\left(K(Z) - \Omega(T)\right)\right] \tag{22}$$

$$W_k' = \hat{W}_k(R)\exp\left[i\left(K(Z) - \Omega(T)\right)\right] \tag{23}$$

$$P' = \hat{P}(R)\exp\left[i\left(K(Z) - \Omega(T)\right)\right] \tag{24}$$

$$\Delta = \Delta_0\exp\left[i\left(K(Z) - \Omega(T)\right)\right] \tag{25}$$

with the amplitude functions $\hat{U}_k(R)$, $\hat{W}_k(R)$ and $\hat{P}(R)$, the initial disturance Δ_0 and the complex functions describing a spatial wave $K(Z) = K_r + iK_i$ and a temporal wave $\Omega(T) = \Omega_r + i\Omega_i$. The real part of the wave

functions describe the oscillation whereas the imaginary parts describe the temporal or spatial growth or decay of a disturbance. The amplitude is a function of the radius R.
From potential theory the pressure oscillation at the gas/liquid interface can be determined as:

$$P_g' = \frac{\rho_g}{\rho_l}\frac{K_1}{K_1'}\left(\Omega_T + \frac{2}{\bar{R}_j}\bar{U}_g + \bar{W}_g K_Z\right)^2 \Delta. \tag{26}$$

with $K_1 = K_1(\bar{R}_j K)$ the modified Bessel function of the second kind of order one and its derivative with respect to R: K_1' and $\Omega_T = \frac{\partial \Omega}{\partial T}$ the derivative of the temporal wave function with respect to time, which is the frequency of the oscillation and $K_Z = \frac{\partial K}{\partial Z}$ the derivative of the spatial wave function with respect to the spatial coordinate which gives the wave number of the oscillation.

Coupling the linear perturbation equations (14) and (17) as well as (15) and (18) at the interaction terms and with the equations (22-25), the linear perturbation equations result in bessels differential equations for the amplitude functions in axial and radial direction. Their solution is subject to the boundary conditions (20 - 21).
Applying the results to equation (19) the dispersion relation for a particle laden dilated viscous liquid jet taking into account the surrounding gas can be written as:

$$\begin{aligned}
&-\frac{(a+b)\,c^2}{a+d}\frac{1}{K_Z}\frac{s^2+K_Z^2}{s^2-K_Z^2}\frac{I_0(K_Z\bar{R}_j)}{I_1(K_Z\bar{R}_j)} = \\
&-\frac{\rho_g}{\rho_l}\frac{K_1(K_Z\bar{R}_j)}{K_Z\,K_0(K_Z\bar{R}_j)+\frac{1}{\bar{R}_j}\,K_1(K_Z\bar{R}_j)}\left\{\Omega_T + \frac{2}{\bar{R}_j}\bar{U}_{g,rel} - K_Z\bar{W}_{g,rel}\right\}^2 - \frac{1}{We}\left[\frac{1}{\bar{R}_j^2} - K_Z^2\right] \\
&+\frac{2}{Re}c\left\{\frac{s^2+K_Z^2}{s^2-K_Z^2}\left(K_Z\frac{I_0\left(K_Z\bar{R}_j\right)}{I_1\left(K_Z\bar{R}_j\right)} - \frac{1}{\bar{R}_j}\right) - \frac{2K_Z^2}{s^2-K_Z^2}\left(s\frac{I_0\left(s\bar{R}_j\right)}{I_1\left(s\bar{R}_j\right)} - \frac{1}{\bar{R}_j}\right)\right\}.
\end{aligned} \tag{27}$$

with the dispersion coefficient $s^2 = K_Z^2 + \frac{(a+b)c}{a}Re$ and the variables $a = i\left(\bar{W}K_Z - \Omega_T\right) + \frac{18}{Re}\frac{\epsilon_f}{D_p^2}\frac{\rho_l}{\rho_s}$, $b = \frac{18}{Re}\frac{\epsilon_s}{D_p^2}$, $c = i\left(\bar{W}K_Z - \Omega_T\right)$ and $d = \frac{18}{Re}\frac{\epsilon_s}{D_p^2}\frac{\rho_l}{\rho_s}$. Distinction is drawn between temporal and spatial development of the disturbances. In temporal stability analysis, a spatial constant wave with wave number $K_{Z,r}$ grows or decays in time. The imaginary part of the spatial wave function is zero. The temporal growth rate $\Omega_{T,i}$ can be determined from the dispersion relation (27). Since the growth rate for a specific wave number changes along the jet because of the elongation of the stationary contour, the growth must be integrated with respect to residence time in temporal analysis. If the temporal growth is positive $\Omega_i = \int_0^{T_{max}} \Omega_{T,i}\, dT > 0$ the wave is temporally unstable. The most unstable wave shows the largest integral growth $\Omega_{i,max}$ and has the critical wave number $K_{Z,r,crit}$.
In spatial stability analysis a temporal constant wave with angular frequency $\Omega_{T,r}$ grows or decays in space with the growth rate $K_{Z,i}$. A wave is unstable if $K_i = \int_0^L K_{Z,i}\, dT < 0$ and the most unstable wave is found at $K_{i,min}$ and has the wave number $K_{Z,r,crit}$.
The resulting drop size can be determined evaluating the wave length $\Lambda = \lambda/r_0 = 2\pi/K_{Z,r}$ and calculate the volume equivalent drop diameter from the time steady solution:

$$D_D = \frac{d_D}{2r_0} = \frac{1}{2}\sqrt[3]{\frac{12\pi}{K_{Z,r,crit}}\bar{R}_j^2|_{Z=L}} \tag{28}$$

for spatial as well as for temporal instability.

Results

The numerical results are compared to experimental results gained by shadow imaging technology. The liquid properties were modified by different mixtures of water and glycerol and the addition of surfactants. As particles, glass beads were used with two different sizes $d_{p1,50,3} = 6.55\mu m$ and $d_{p2,50,3} = 22.5\mu m$ and with a volume concentration ranging from $\epsilon_s = 0.045$ to $\epsilon_s = 0.2$. The liquid density ranged from $998kg/m^3 < \rho_l < 1234kg/m^3$, the viscosity ranged from $10^{-3}Pas < \eta_l < 0.14Pas$ and the surface tension $3\cdot 10^{-2}N/m < \sigma < 7.2\cdot 10^{-2}N/m$. The breakup length was determined experimentally and serves as boundary condition for the calculation.

Numerical results and experimental verification

The motivation of this work is the calculation of the drop size, that results from the Rayleigh type jet breakup of a rotating particle laden liquid jet. Decisive are therefore the jet contour from time steady motion as well as the

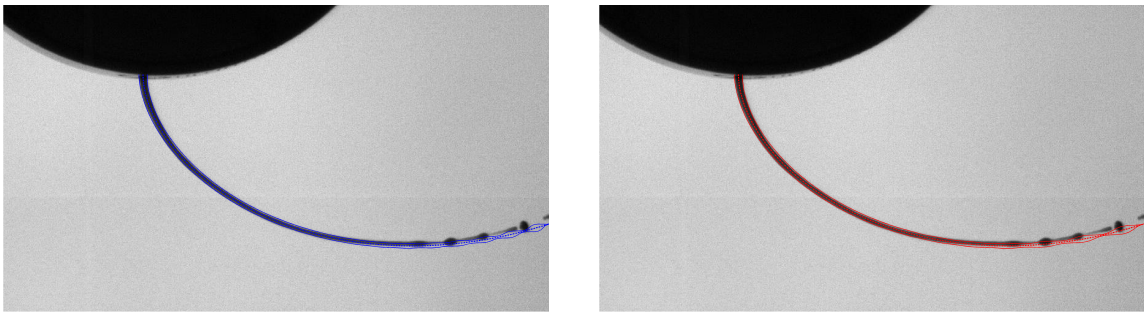

Figure 2. Experimentally gained and calculated (coloured overlay) perturbed jet contour from temporal stability analysis (left) and spatial stability analysis (right); water, $w_0 = 0.93$ m/s, $\omega = 30$ rad/s, $n_0 = 60$ mm, $r_0 = 1$ mm.

stability analysis. The comparison between the experimentally gained jet contour with the calculation can be seen in figure 2 for temporal stability analysis (left) and spatial stability analysis (right). A jet consisting of pure water emitted with an exit velocity of $w_0 = 0.93$ m/s from a nozzle with a radius of $r_0 = 1$ mm. The rotating atomizer has a radius of $n_0 = 60$ mm and rotates with an angular velocity of $\omega = 30$ rad/s. The time steady trajectory as well as the contraction of the jet are in good accordance with the photograph. Interesting is the comparison of the oscillation of the jet radius from spatial and temporal stability stability analysis. The critical values for the wave lengths are shown respectively. The resulting critical wave length from temporal stability analysis is decisively shorter compared to the one gained by spatial stability analysis and the one observed in the experiment. This is distinguishable from the maxima of the oscillation of the jet diameter which are much closer than those from the experiment in the breakup zone (figure 2, left). The critical wave length resulting from spatial stability analysis is in good accordance to the experimental observation (figure 2, right). The exact contour in the breakup zone in particular the formation of small ligaments between two main droplets are perturbations of higher order and thus can not be expressed by linear stability analysis. The resulting drop size from the experiment ($d_{50,3}$) gained by shadow imaging technology is $D_{T,exp} = 1.22$, from spatial stability analysis results a drop size of $D_{T,sp} = 1.31$ and from temporal stability analysis $D_{T,temp} = 1.09$ is determined. Thus, the experimentally observed drop size is remarkably lower than the one resulting from spatial stability analysis, even though the visible results concerning the wave length of the oscillations are in good accordance. Assuming also good accordance in the time steady solution, the differences in resulting drop size can be explained by the occurance of smaller satellite droplets. A further explanation for the smaller droplets in the experiment is that due to gravity, the jet is dropping from the imaging level and thus the droplets on the photograph appear smaller than they are.

Drop Size

The drop size from the model is compared to experimental results gained by shadow imaging technology. Figure 3 shows the scaled drop size $D_T = d_t/d_0$ for different Weber numbers We as a function of rotation number, which was varied in a range of $10^{-3} \leq Ro \leq 10$. The diameter ratio as well as the Ohnesorge number $Oh = \sqrt{We}/Re$ was kept constant at $D = 60$ and $Oh = 0.033$. The results were gained for a pure liquid, thus $\epsilon_s = 0$. The calculated results from temporal (solid) and spatial (dashed) stability analysis are compared to the experimental results (symbols).

Even though the rotation number Ro is not contained in the dispersion relation explicitly, the calculated drop size from temporal as well as from spatial stability analysis is decreasing with increasing rotation number. Centrifugal acceleration and thus elongation of the jet results in smaller jet diameters from time steady motion $\bar{R}_j$ in the breakup zone and therefore results in smaller droplets (compare equation (28)).

The calculated drop sizes from spatial stability analysis are higher by trend compared to those resulting from temporal stability analysis. For very small rotation numbers, both the results from temporal as well as from spatial stability analysis tend towards $D_T = 1.89$, the solution found from [15, 19] for jets without contraction.

With increasing Weber number We and constant rotation number Ro, smaller drop sizes are observed. This can be explained by the increase in jet length with increasing Weber number. Long jets are exposed to the centrifugal force over a longer period of time which leads to thinner jets in the breakup zone.

For high Weber numbers $We = 100$ and high rotation numbers $Ro \geq 1$ numerical difficulties in the solution of equation (27) occur. The decrease of drop size with increasing rotation number as well as with increasing Weber

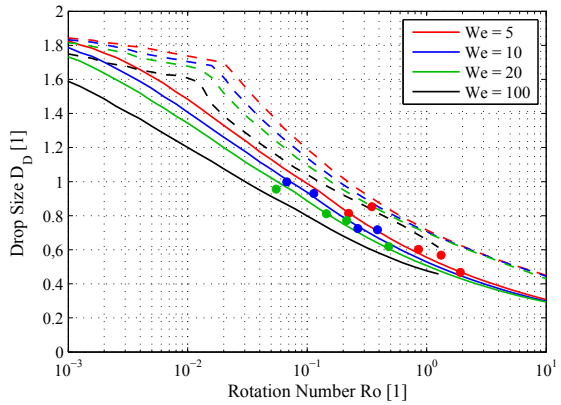

Figure 3. Scaled drop size vs. rotation number for different Weber numbers; $D = 60$, $Oh = 0.033$, $\epsilon_s = 0$, solid lines: results from temporal stability analysis, dashed lines: results from spatial stability analysis, symbols: experiments.

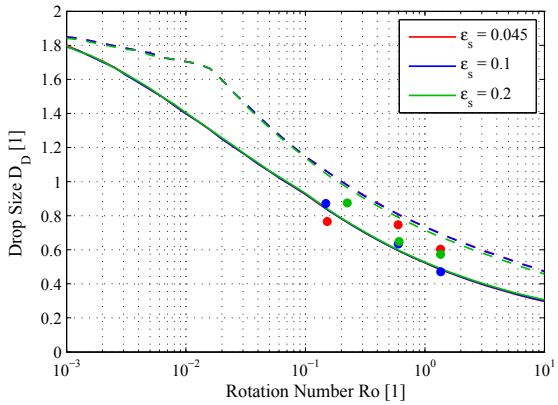

Figure 4. Scaled drop size vs. rotation number for different particle concentrations ϵ_s; $Re = 63$, $We = 10$, $D = 60$, $\rho_s/\rho_l = 0.88$, $D_p = 0.0086$, solid lines: results from temporal stability analysis, dashed lines: results from spatial stability analysis, symbols: experiments.

number are also observed in the experiment. By trend, the results from temporal stability analysis are closer to the experimentally gained ones compared to the results from spatial instability analysis. As explained above, this is due to the occurance of satellite droplets as well as insufficient shadow imaging technology.
The following discussion is about particle laden liquids with a 60w% glycerol solution as continuous phase. Figure 4 shows the scaled drop size as a function of rotation number Ro for different particle concentrations. The parameters Reynolds number, Weber number, diameter ratio, density ratio of solid particles to liquid are constant. Both temporal as well as spatial stability analysis do not show a significant effect on the resulting drop size due to different particle concentrations. The lines are over the whole investigated span of rotation numbers congruent. The results from the experiment do not show a significant trend either. They are by trend closer to the results from spatial stability analysis compared to figure 3. In the experiments we observed less formation of satellite droplets for particle laden liquids. Thus, the evaluated representative drop size is higher.

Concluding remark

A physical-mathematical model is presented for the determination of the drop size obtained by rotational atomization in the Rayleigh breakup regime of particle laden liquid jets. The influence of the surrounding gas is considered in both the time steady motion and the stability analysis. The breakup length was determined by experimental data and serves as a boundary condition for the model. The comparison between experimental findings and numerical solutions shows the models' capability of calculating the drop sizes of particle laden liquids. However, the influence of the particulate matter was found to be irrelevant in the investigated parameter range. The model promises the forecast of drop sizes and is in good accordance to the experimental findings.

Acknowledgements

This project is part of the "'process spray"' SPP1423 of the german research foundation DFG. The authors are grateful for funding.

Nomenclature

Roman symbols

d	Diameter (m)
k	Curvature radius (m)
K	Spatial wave function
n	Position vector (m)
p	Pressure (Pa)
r	Radial coord., radius (m)
s	Dispersion parameter
t	Time (s)
u	Radial velocity ($\mathrm{m\,s^{-1}}$)
v	Velocity vector ($\mathrm{m\,s^{-1}}$)
w	Axial velocity ($\mathrm{m\,s^{-1}}$)
z	Axial coordinate (m)
$c_{D,lg}$	Drag coefficient of jet
We	Weber number
Re	Reynolds number
Ro	Rotation number
D	Diameter ratio
H	Viscosity function
T	Time

Greek symbols

α	Inclination angle
δ	Radial Displacement (m)
Δ	Dim.-less Radial Displ.
η	Viscosity (Pa s)
φ	Angular coordinate
ζ	Angle of incident gas flow
ρ	Density ($\mathrm{kg\,m^{-3}}$)
ϵ	Volume concentration
κ	Constant
σ	Surface tension ($\mathrm{N\,m^{-1}}$)
λ	Wave length (m)
ω	Angular velocity ($\mathrm{rad\,s^{-1}}$)
Ω	Temporal wave function

Subscripts

0	Condition at orifice
1	Substitution
crit	Critical
max	Maximum
min	Minimum
rel	Relative
c	Centrifugal
D	Drop
g	Gas
i	Imaginary
j	Jet
l	Liquid
p	Particle
r	Real
s	Solid
T	Deriv. with respect to T
Z	Deriv. with respect to Z

References

[1] D. B. Bogy. Breakup of a liquid jet: third perturbation cosserat solution. *Phys. Fluids*, 22:224–230, 1979.

[2] S. Chandrasekhar. *Hydrodynamic and Hydromagnetic Stability*. Dover Pubn. Inc., 1981 edition, 1981.

[3] S. P. Decent, A. C. King, M. J. H. Simmons, E. I. Părău, I. M. Wallwork, C. J. Gurney, and J. Uddin. The trajectory and stability of a spiralling liquid jet: Viscous theory. *Appl. Math. Modelling*, 33:4283 – 4302, 2009.

[4] S. Gramlich. *Numerische und experimentelle Untersuchungen zum Zerfall feststoffbeladener Flüssigkeitsstrahlen im Zentrifugalfeld*. PhD thesis, University of Stuttgart, 2011.

[5] S. Gramlich, A. Mescher, M. Piesche, and P. Walzel. Modellierung und experimentelle untersuchung des gasinduzierten zerfalls gedehnter flüssigkeitsstrahlen im erdschwerefeld. *Chemie Ingenieur Technik*, 83:273 – 279, 2011.

[6] S. Gramlich and M. Piesche. The instability of particle laden spiralling liquid jets. In *Proceedings of 7th international conference on multiphase flow*, Tampa, Fl, USA, 2010.

[7] S. Gramlich and M. Piesche. Physikalisch-mathematische und experimentelle untersuchungen zum zerfall laminarer flüssigkeitsstrahlen im zentrifugalfeld. In *Proceedings, Spray 2010*, Heidelberg, 2010.

[8] J. B. Keller, S. I. Rubinow, and Y. O. Tu. Spatial instability of a jet. *Phys. Fluids*, 16:2052–2055, 1973.

[9] Y. Kitamura, K. Egawa, and T. Takahashi. Drop formation from liquid jet ejected from a rotating nozzle. *J. Chem. Eng. Japan*, 10:1–5, 1977.

[10] A. Mescher, S. Gramlich, M. Piesche, and P. Walzel. Modelling and numerical simulation of the gas-induced break-up of liquid threads stretched by gravity. *Chem. Eng. Tech.*, 34:921 – 926, 2011.

[11] S. Nonnenmacher and M. Piesche. Stability behavior of liquid jets under gravity. *Chem. Eng. Tech.*, 27(5):529–536, 2004.

[12] M. Piesche, M. Breitling, and S. Schütz. Zeitliche und räumliche hydrodynamische Instabilitäten feststoffbeladener Flüssigkeitsstrahlen. *Chem. Ing. Tech.*, 77(6):742–747, 2005.

[13] W. T. Pimbley and H.C. Lee. Satellite droplet formation in a liquid jet. *IBM J. Res. Develop.*, 21:21–30, 1977.

[14] E. I. Părău, S. P. Decent, M. J. H. Simmons, D. C. Y. Wong, and A. C. King. Nonlinear viscous liquid jets emerging from a rotating orifice. *J. Eng. Math.*, 57:159–179, 2007.

[15] Lord Rayleigh. On the instability of jets. *Proc. London Math. Soc.*, 10:4–12, 1878.

[16] Lord Rayleigh. On the capillary phenomena of jets. *Proc. London Math. Soc.*, 29:71–97, 1879.

[17] S. Sauter. *Globale Stabilität schlanker schweregetriebener hochviskoser und viskoelastischer Flüssigkeitsstränge*. Dissertation, Universität Karlsruhe (TH), 2005.

[18] I. M. Wallwork, S. P. Decent, A. C. King, and R. M. S. M. Schulkes. The trajectory and stability of a spiralling liquid jet. part 1. inviscid theory. *J. Fluid Mech.*, 459:43–65, 2002.

[19] C. Weber. Zum Zerfall eines Flüssigkeitsstrahles. *ZAMM*, 11:136–154, 1931.